Localization of atomic excitation beyond the diffraction limit using electromagnetically induced transparency

J. A. Miles, Diptaranjan Das, Z. J. Simmons, and D. D. Yavuz
Department of Physics, University of Wisconsin, 1150 University Avenue, Madison, Wisconsin 53706, USA
(Received 2 July 2015; published 21 September 2015)

We experimentally demonstrate the localization of excitation between hyperfine ground states of ^{87}Rb atoms to as small as $\lambda/13$-wide spatial regions. We use ultracold atoms trapped in a dipole trap and utilize electromagnetically induced transparency (EIT) for the atomic excitation. The localization is achieved by combining a spatially varying coupling laser (standing wave) with the intensity dependence of EIT. The excitation is fast (150 ns laser pulses) and the dark-state fidelity can be made higher than 94% throughout the standing wave. Because the width of the localized regions is much smaller than the wavelength of the driving light, traditional optical imaging techniques cannot resolve the localized features. Therefore, to measure the excitation profile, we use an autocorrelation-like method where we perform two EIT sequences separated by a time delay, during which we move the standing wave.

DOI: 10.1103/PhysRevA.92.033838 PACS number(s): 42.50.Gy, 42.25.Kb, 32.80.Qk

I. INTRODUCTION

The diffraction limit, which posits that traditional optical techniques cannot resolve or write features smaller than about half the wavelength of light, is an important barrier for a variety of research areas. For example, a number of quantum computing implementations, such as those utilizing trapped neutral atoms, use focused laser beams to trap, initialize, and manipulate qubits [1–5]. In a neutral-atom quantum computing architecture, the qubit spacing has to be larger than half the wavelength, which limits the two-qubit interaction energies that can be obtained (for example through Rydberg dipole-dipole interaction). The necessary qubit spacing in turn limits the fidelity and the speed of the two-qubit gates. A technique to address atoms with high fidelity in subwavelength spatial scales would greatly improve the performance of the two-qubit gates. In this work, we use the dark state of electromagnetically induced transparency (EIT) [6–9] to address atoms in regions much smaller than the diffraction limit. We use a standing-wave coupling laser and demonstrate efficient transfer between the ground levels of ^{87}Rb in regions with widths as small as $\lambda/13$. The transfer is fast (150 ns laser pulses) and the fidelity for the atomic system to be in the dark state can be made higher than 94% at all spatial points along the standing wave. We perform these experiments using ultracold ^{87}Rb atoms trapped in a far-off-resonant dipole trap at a temperature of ≈ 1 μK. Although other techniques have been investigated that achieve subwavelength resolution, using the dark state provides key advantages for quantum computing. The atoms are coherently transferred [9], keeping their phase relationship with other qubits intact. The dark state can be prepared with little population transfer to a radiative excited state, which reduces heating and decoherence from spontaneous emission. Because the excitation is coherent, dark-state-based localization can be achieved using short and intense laser pulses, allowing fast quantum gates to be constructed.

There has been other important work related to addressing atoms with a resolution that is not limited by diffraction. Biological imaging at the nanoscale is now a mature field with a number of demonstrated techniques such as stimulated-emission depletion (STED) microscopy [10,11]. Thomas and colleagues have experimentally demonstrated subwavelength localization of atomic excitation using spatially varying energy shifts of the atomic levels [12–15]. Localization using resonance fluorescence, spectroscopic measurements, and measurement-induced diffraction have also been discussed [16–27]. Recently, subwavelength addressing of individual sites in an optical lattice has been demonstrated using spatially varying light shift and microwave transfer [28]. All of these techniques are related in the sense that they utilize some type of nonlinear atomic response to the interacting light. As we will discuss below, dark-state-based localization utilizes the nonlinear dependence of the state vector to the intensity of the coupling laser beam. Starting from the ground state of the atomic system, the dark state can be prepared adiabatically by using a counterintuitive pulse sequence; i.e., the coupling laser is turned on before the probe laser. With the system prepared adiabatically, the excited-level population can be made very small resulting in suppressed spontaneous emission and decoherence.

II. LOCALIZATION USING THE DARK STATE OF ELECTROMAGNETICALLY INDUCED TRANSPARENCY

Localization of atomic excitation using the dark state was first proposed by Agarwal and colleagues [29], and was later expanded by our group [30] as well as Lukin and coworkers [31]. Detailed investigations of interaction time of the lasers and population redistribution between hyperfine levels in dark-state-based localization have recently been carried out by Elliott and colleagues [32]. The first experiment that observed dark-state-based localization was performed in a vapor cell by Scully and colleagues [33]. About 4 years ago, we reported a proof-of-principle experiment that demonstrated dark-state-based localization using ultracold atoms trapped inside a magneto-optical trap (MOT) [34]. This experiment suffered from a number of technical disadvantages such as the high atomic temperatures and large spatial extent of the MOT. We recently extended this experiment to atoms trapped in a dipole trap and observed excitation localization to regions 100 nm wide (about $\lambda/8$) [35]. Our current experiment is an extension of this recent work with the following improvements: (i) We

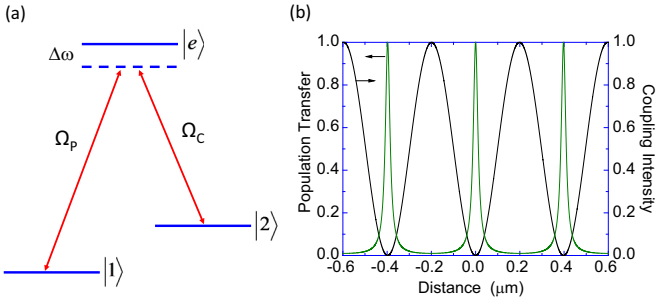

FIG. 1. (Color online) (a) An EIT Λ scheme where the probe and coupling laser beams with Rabi frequencies Ω_P and Ω_C interact with a three-level atomic system. Starting from the ground state, atoms can be adiabatically prepared into the dark state by turning on the coupling laser before the probe laser beam. The quantity $\Delta\omega$ is the single-photon detuning of both lasers from the excited level. (b) An EIT-based localization scheme where Ω_P is constant and Ω_C is a spatially varying standing wave. Population is most efficiently transferred to state $|2\rangle$ near the nodes of the standing wave with $\Omega_C \approx 0$.

use a dipole trap laser at a wavelength of 1.064 μm (instead of 850 nm), which results in considerably less heating of the atoms due to photon scattering from the trapping beam. As a result, we can evaporatively cool the atoms to temperatures below 1 μK, which greatly increases the resolution of our measurement protocol. (ii) We transfer the atoms using the D_1 line instead of the D_2 line of ^{87}Rb. This reduces the influence of other excited-state hyperfine levels during the EIT process. (iii) Additionally, we explore EIT both on resonance and slightly off single-photon resonance, as well as investigate the dark-state fidelity everywhere along the coupling laser standing wave. Incorporating these improvements and extensions, we have been able to infer spatial features as small as 60 nm ($\lambda/13$) and also demonstrate 70-nm-wide features with dark-state fidelity exceeding 94%.

The simplified energy level diagram is shown in Fig. 1. Two laser pulses designated as the coupling beam (with Rabi frequency Ω_C) and the probe beam (Ω_P) interact with a three-level atomic system. The two lower states, states $|1\rangle$ and $|2\rangle$, are metastable with long lifetimes, and they are coupled to each other through the radiative excited state $|e\rangle$. The atoms are initialized into state $|1\rangle$ before applying a counterintuitive pulse sequence where the coupling laser is turned on before the probe beam. For sufficiently intense laser beams turning on sufficiently slowly, this ensures adiabatic preparation of the atomic system into the dark state which is given by [9]

$$|\psi_{\text{dark}}\rangle = \frac{\Omega_C^*}{\sqrt{|\Omega_P|^2 + |\Omega_C|^2}}|1\rangle - \frac{\Omega_P^*}{\sqrt{|\Omega_P|^2 + |\Omega_C|^2}}|2\rangle . \quad (1)$$

A critical feature of the dark state is that there is no contribution from the excited state $|e\rangle$. From Eq. (1), the populations of states $|1\rangle$ and $|2\rangle$ are determined by the Rabi frequencies, and therefore the intensities of the two lasers. The probability that an atom is transferred into $|2\rangle$ by an EIT pulse sequence is $|\langle 2|\psi_{\text{dark}}\rangle|^2 = |\Omega_P|^2/(|\Omega_C|^2 + |\Omega_P|^2)$, and increases as the ratio $|\Omega_C|^2/|\Omega_P|^2$ decreases. The population of state $|2\rangle$ can then be tightly localized if the coupling laser goes through an intensity minimum. As suggested by Refs.

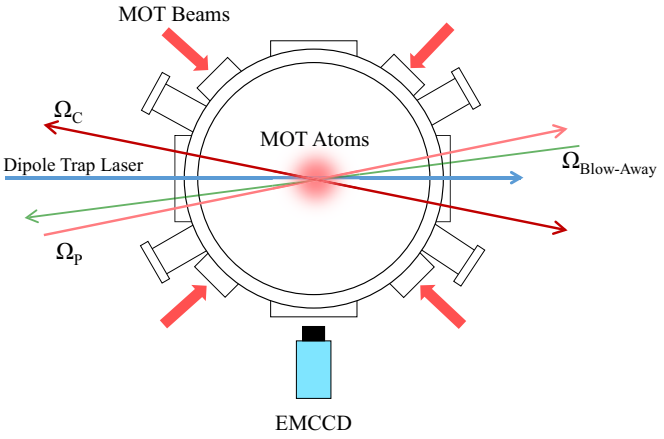

FIG. 2. (Color online) The top view of the vacuum chamber and simplified experimental schematic of the laser beams. The probe and coupling laser beams propagate at a slight angle to the far-off-resonant dipole-trap (FORT) laser. The coupling standing wave is produced using a counterpropagating beam pair. An electron-multiplying CCD camera (EMCCD) images the remaining atoms left in the FORT after an EIT experiment. The laser $\Omega_{\text{blow-away}}$ is used for the measurement protocol, and heats and removes any atoms that are in the $F = 2$ level after the experimental pulse sequence.

[29,31], an easy approach to produce a spatially varying coupling laser is to use a standing wave. This setup is demonstrated in Fig. 1 where the atoms are transferred to state $|2\rangle$ only near the nodes of the coupling standing wave and otherwise remain in state $|1\rangle$. This plot is representative of the atomic population after a single EIT pulse and assumes a spatially invariant probe laser (i.e., constant Ω_P). As we will discuss below, to measure the transfer profile to state $|2\rangle$, we will use a sequence of two EIT pulses and move the coupling laser standing wave to a new position for the second pulse.

III. EXPERIMENTAL PROCEDURE

The simplified experimental setup is shown in Fig. 2. The experiment is performed in a 14-port stainless-steel ultrahigh-vacuum chamber at a pressure of about 5×10^{-9} torr. The MOT is generated from three retroreflected beams each having 50 mW of power with a beam diameter of 3 cm. All three beams originate from a semiconductor tapered amplifier which is seeded by a custom-built external-cavity diode laser (ECDL). The ECDL is locked to the D_1 line of ^{87}Rb near a wavelength of 795 nm using saturated absorption locking. The far-off-resonance trap (FORT) for the atoms is formed using a 1064 nm diode-pumped solid-state (DPSS) laser that produces up to 20 W of power. The FORT beam is focused to a $1/e^2$ beam radius of 25 μm and is overlapped with the MOT. The initial depth of the FORT potential is about 0.5 mK. Once the atoms are trapped in the FORT, they are evaporatively cooled down to a temperature below 1 μK by reducing the FORT potential depth to $\approx$10 μK. Evaporative cooling is performed over about 200 ms. At the end of evaporative cooling, the number of atoms trapped in the FORT is a few thousand.

The coupling and probe lasers are both generated from the same master ECDL. Semiconductor tapered amplifiers and high-frequency acousto-optic modulators are then used

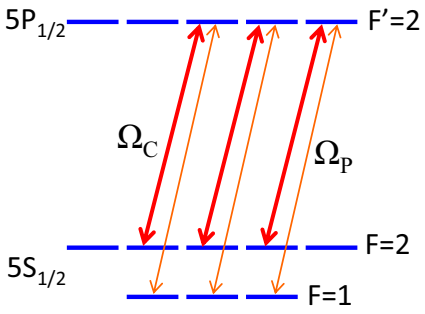

FIG. 3. (Color online) The relevant energy level structure of ^{87}Rb. The probe and coupling lasers form an EIT Λ scheme by coupling the $F = 1 \rightarrow F' = 2$ and $F = 2 \rightarrow F' = 2$ transitions in the D_1 line. The atoms are first initialized to the $F = 1$ level and are transferred to $F = 2$ through three parallel m-level channels. For on resonance experiments, the atoms are pumped into $m_F = 0$ state and a single EIT channel is used. See text for details.

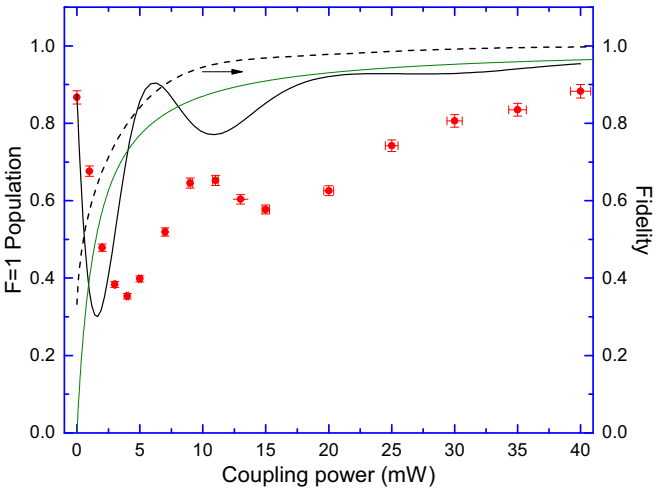

FIG. 4. (Color online) The population remaining in the $F = 1$ level after a single EIT pulse as the coupling laser power is varied. This experiment is performed using a single coupling laser; i.e., there is no standing wave. The solid black line is the result of numerical simulations of the density matrix without any adjustable parameters; i.e., all the beam parameters that are used are experimentally measured. The solid green line shows the $F = 1$ level population using the ideal dark state solution of Eq. (1). Both the experimental data and the numerical simulations show oscillations due to nonadiabatic corrections to the dark state. The dotted line is the fidelity of dark-state preparation, which is a measure of the distance between the density matrix calculated in the simulations and the ideal dark state density matrix. For a coupling laser power of 40 mW, the calculated coupling Rabi frequencies for the three channels are $\Omega_C = 18.2\Gamma$ ($m_F = -1 \rightarrow m_{F'} = 0$), $\Omega_C = 18.2\Gamma$ ($m_F = 0 \rightarrow m_{F'} = 1$), and $\Omega_C = 14.9\Gamma$ ($m_F = 1 \rightarrow m_{F'} = 2$).

to produce the required frequency spacing of 6.834 GHz and sufficient optical power in each beam. Further details regarding our laser system can be found in our previous publications [34–36]. As shown in Fig. 3, the two lasers form an EIT Λ scheme by coupling the $F = 1 \rightarrow F' = 2$ and $F = 2 \rightarrow F' = 2$ transitions in the D_1 line of ^{87}Rb. The decay rate of the excited $5P_{1/2}$ level is $\Gamma = 2\pi \times 5.75$ MHz. The polarizations of the two beams are linear but orthogonal to one another, which allows atoms to transfer between identical ground-state m levels via an $m' = m \pm 1$ excited state (with the quantization axis chosen along the propagation direction of the probe laser beam). The atoms are initialized in the $F = 1$ level and then transferred to $F = 2$ through three parallel m-level channels.

IV. OFF-RESONANCE EXPERIMENTAL RESULTS

A. EIT with a single coupling laser beam

In our experiments, we first investigated EIT using a single coupling laser (i.e., there is no standing wave). Specifically, we explored the population transfer due to EIT as the power of the coupling beam is varied. These investigations are indicative of the expected spatial profiles when the standing wave is present. In this section, we will discuss in detail our off-resonant EIT experiments, performed $\Delta\omega = 5.2\Gamma = 30$ MHz away from the single-photon resonance. Consistent with our numerical simulations which we will discuss below, we have found this configuration to produce fairly complex excitation profiles with feature sizes as small as 60 nm. The experiments are performed using coupling and probe beams with pulse widths of 150 ns and 100 ns, respectively. To prepare the atomic system adiabatically, the coupling laser is turned on before the probe, and both lasers are turned off simultaneously. The beams have collimated $1/e^2$ beam radii of 0.8 mm (coupling) and 1.3 mm (probe), large compared to the size of the atomic cloud. The frequencies of both of the laser beams are positioned 30 MHz away from single-photon resonance ($F' = 2$ level in $5P_{1/2}$) to reduce probe optical pumping. As a result, only when both probe and coupling lasers are turned on, the atoms are efficiently transferred from $F = 1$ to $F = 2$. This, in turn, gives us confidence that the population transfer is coherent. The optical power of the probe laser beam is set to a constant value of 3.5 mW. The calculated probe laser Rabi frequencies for the three channels are $\Omega_P = 1.95\Gamma$ ($m_F = -1 \rightarrow m_{F'} = 0$), $\Omega_P = 3.33\Gamma$ ($m_F = 0 \rightarrow m_{F'} = 1$), and $\Omega_P = 4.71\Gamma$ ($m_F = 1 \rightarrow m_{F'} = 2$), respectively. We first experimentally determined what percentage of atoms transfer to $F = 2$ after a single EIT pulse using only one coupling beam. After the EIT pulse, the blow-away beam ($\Omega_{\text{blow-away}}$) with a saturation parameter of $s = 22$ heats the $F = 2$ atoms leaving only $F = 1$ atoms in the FORT. The experimental arrangement of the lasers is pictured in Fig. 2.

In Fig. 4, we measure the percentage of atoms in the $F = 1$ level as we vary the coupling laser beam power from 0 to 40 mW. For a coupling laser power of 40 mW, the calculated coupling Rabi frequencies for the three channels are $\Omega_C = 18.2\Gamma$ ($m_F = -1 \rightarrow m_{F'} = 0$), $\Omega_C = 18.2\Gamma$ ($m_F = 0 \rightarrow m_{F'} = 1$), and $\Omega_C = 14.9\Gamma$ ($m_F = 1 \rightarrow m_{F'} = 2$), respectively. At low coupling intensities, the EIT pulse is so short that the system does not have sufficient time to reach the dark state, resulting in low atomic transfer to the $F = 2$ level. Because of the pulsed nature of excitation, we cannot assume that the populations will exactly follow the analytical solution of Eq. (1). We simulate the experimental data by numerically solving the density matrix equations for each parallel m-level EIT channel (Fig. 3). We then average over the three possible channels assuming that the atoms are

initially evenly distributed across the three m levels. The solid black line in Fig. 4 shows the result of the numerical simulation as the coupling laser power is varied without any adjustable parameters; i.e., all the beam parameters are experimentally measured and we use the well-known transition matrix elements from the literature [37]. Comparing the two plots shows good qualitative agreement but a substantial quantitative difference between the simulations and the experimental data. In particular, the simulations predict that the population in the $F = 1$ level should be at a minimum (i.e., the transfer to the $F = 2$ level should be at a maximum) at a substantially lower coupling laser optical power. One explanation could be a spatial misalignment of the coupling laser beam from the FORT atoms. For comparison, the solid green line shows the population of the $F = 1$ level using the ideal dark state equation of Eq. (1). Both the experimental data and the numerical simulations show oscillations as the coupling laser power is increased. These oscillations are due to nonadiabatic corrections to the evolution of the atomic system.

Since it is clear that there are significant corrections to the dark state for the experimental conditions of Fig. 4, it is important to evaluate the fidelity of dark-state preparation. For this purpose we calculate $\mathrm{Tr}(\sqrt{\sqrt{\sigma}\rho\sqrt{\sigma}})$ (Tr stands for the matrix trace operation) where σ is the density matrix of the dark state from Eq. (1) and ρ is the density matrix that we calculate from our simulations [1]. The dotted line in Fig. 4 shows the fidelity of dark-state preparation as the coupling laser power is increased. The dark-state preparation fidelity increases with increasing coupling beam power. This is expected since the separation of the eigenvalues of the Hamiltonian scales with the coupling laser Rabi frequency.

B. Autocorrelation measurement protocol

In this section, we discuss the localization experiments in detail. As mentioned before, we use an autocorrelation-like technique to determine the spatial profiles of the atomic populations. The exact protocol is described in depth in Ref. [35] and will be summarized here. We use two EIT transfer sequences separated by time τ. Two counterpropagating lasers produce the coupling beam standing wave and the frequencies of these two beams are set to be slightly different by an amount δf. The coupling beam intensity varies as $I_C(x) \sim |\Omega_C|^2 \sin^2(2\pi x/\lambda)$ where x is the position along the FORT and $\lambda = 795$ nm. The first EIT pulse transfers atoms to the $F = 2$ level depending on the coupling laser intensity at that specific position. After the first EIT pulse, the blow-away laser is turned on and interacts with only the $F = 2$ atoms through the $F = 2 \rightarrow F' = 3$ cycling transition of the D_2 line. This laser heats the atoms that are in the $F = 2$ by photon recoil ejecting them from the trap. The blow-away laser is only on between the two EIT pulses. During this time the standing wave is shifted by an amount $\delta x = \delta f \tau(\lambda/2)$ because of the small frequency difference between the two beams. At this point the second EIT pulse is applied to the atoms. The number of atoms the second EIT pulse transfers to $F = 2$ level depends on the new position of the standing wave compared to its original position (i.e., its position during the first EIT pulse). After the second EIT pulse, the blow-away beam is turned on again, heating up any atoms that the second EIT pulse has transferred to $F = 2$. The total number of atoms that remain in the $F = 1$ level are then measured with the EMCCD through a laser-induced fluorescence measurement using the cycling transition. The whole procedure is repeated for many different values of δf and as a result, a correlation between the excitation profiles generated by the two EIT pulses is recorded. This correlation measurement enables us to infer the spatial profile of the excitation that results from a single EIT pulse. For this technique to work the atoms must be cold enough that the initial imprinted profile does not spread too much between the two EIT pulses.

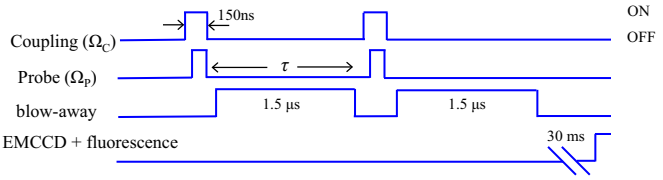

FIG. 5. (Color online) Timing of the autocorrelation experiment protocol. After evaporatively cooling the FORT atoms for 200 ms, the first EIT pulse sequence is turned on, transferring some atoms to the $F = 2$ level. The blow-away beam heats the atoms that have been transferred, ejecting them from the trap. The procedure is repeated with the second EIT pulse, after which the remaining ($F = 1$) atoms in the trap are imaged with a laser-induced fluorescence measurement.

Figure 5 shows the timing diagram of such a correlation measurement. The procedure begins with loading the MOT for 350 ms. The 1064 nm FORT laser beam is turned on for 50 ms while the MOT beams are simultaneously detuned and attenuated, cooling the atoms further through polarization gradient cooling. During this time the MOT repumper beam is also attenuated to maximize loading into the FORT. The atoms that are trapped in the FORT are then evaporatively cooled by reducing the trap depth to $\approx$10 μK over a period of 200 ms. The temperature of the atoms at the end of evaporative cooling is below 1 μK. With the atoms evaporatively cooled, the two counterpropagating coupling beams are turned on with pulse widths of 150 ns. The probe beam is then turned on for the last 100 ns to overlap with the coupling lasers. After the EIT pulse, the blow-away beam is turned on for a duration of 1.5 μs to heat the atoms that have been transferred to the $F = 2$ level. The EIT pulse followed by the blow-away beam cycle is repeated again with the standing wave moved to a different position as described above.

C. Correlation experimental results

Figures 6(a) and 6(b) show experimental correlation traces as the frequency difference between the two beams δf (and therefore the movement distance of the standing wave δx) is scanned. Here coupling laser power in the standing wave ranges from 0 to 10 mW and 0 to 20 mW, respectively. This data are recorded over a scanning distance of approximately two periods of the standing wave. The pattern begins to repeat itself, as expected, when the scanning distance δx is a multiple of $\lambda/2 = 397.5$ nm. At $\delta x = 0$ the standing wave has not moved between the two EIT pulses and relatively few atoms should be transferred to the $F = 2$ level during the second EIT

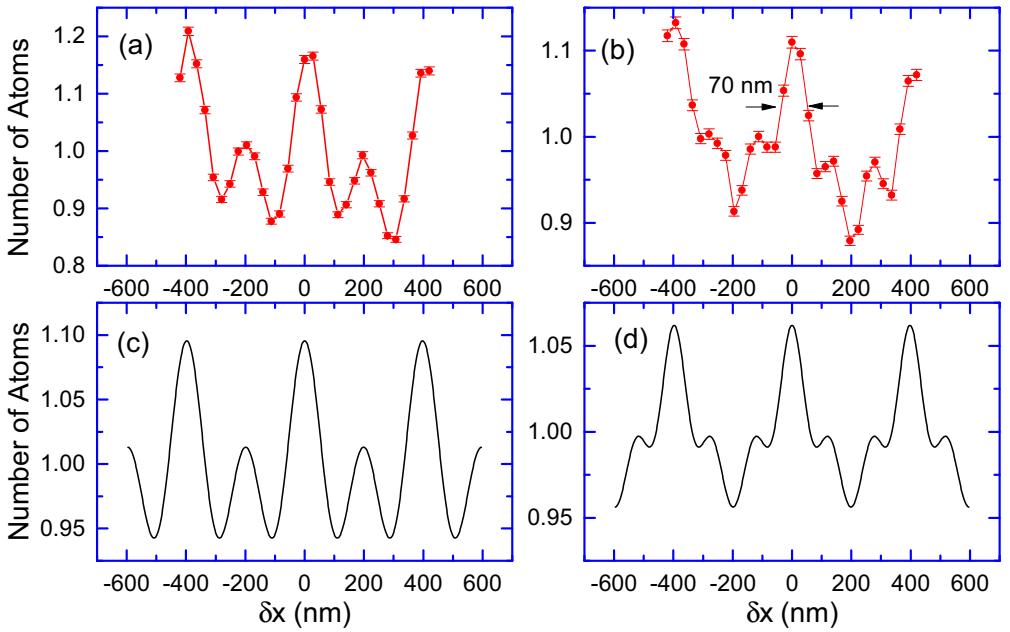

FIG. 6. (Color online) The number of atoms that remain in the trap as a function of scanning distance of the standing wave δx. The coupling laser power in the standing wave ranges from (a) 0 to 10 mW, and (b) 0 to 20 mW, respectively. As expected, the correlation traces are periodic with a period of half the wavelength, $\lambda/2 = 397.5$ nm, and their maxima are lined up with $\delta x = 0$. (c) and (d) show the numerical simulations of the density matrix with a single adjustable fitting parameter, which is the power of the coupling standing wave. These simulated correlation traces were generated using the single EIT sequence transfer profiles that are displayed in Fig. 7. See text for more details.

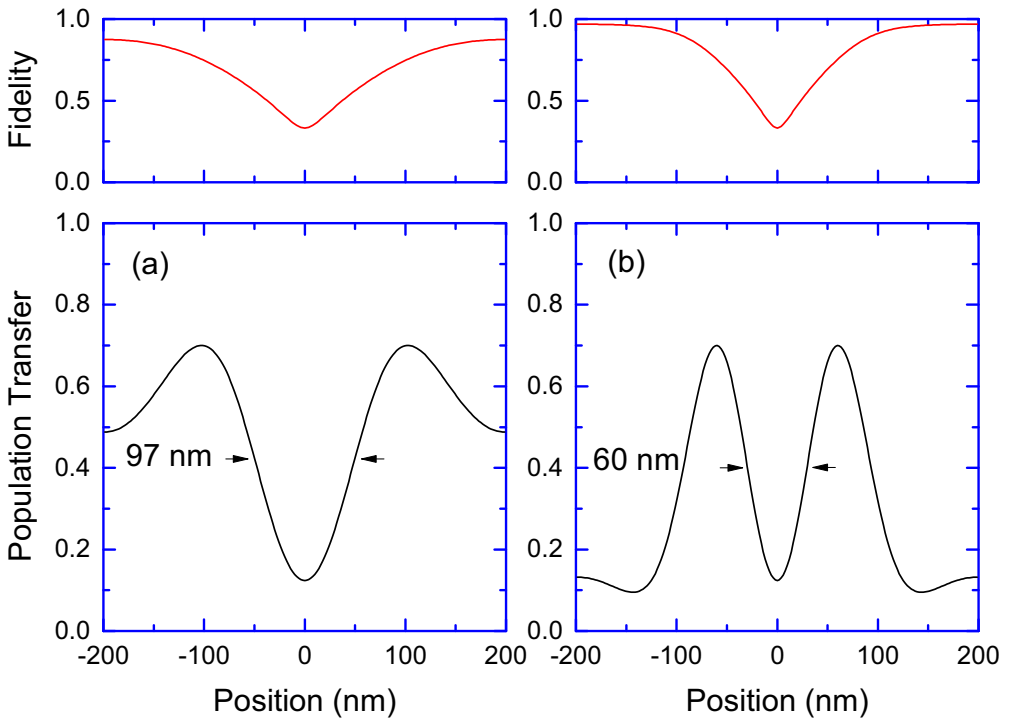

FIG. 7. (Color online) The density matrix simulation of the inferred population transfer to the $F = 2$ level as a function of the position in the standing wave for a coupling power range of (a) 0 to 3 mW and (b) 0 to 7.5 mW. "0" in the horizontal axis coincides with the intensity minimum of the standing wave and the results are displayed over one period. These simulations produce the correlation traces that agree well with the experimental results as shown in Fig. 6. In (b), the middle feature has a width of 60 nm or $\lambda/13.3$, a factor of 6.6 better than the diffraction limit. The top plots show the calculated fidelity of the system to be in the dark state. At the nodes, the fidelity drops to a low value of 33% since the coupling intensity vanishes at these points.

pulse. As a result a maximum in the total number of remaining atoms is expected when $\delta x = 0$, which is observed in both of the experimental plots. The correlation traces show features with full-width-half-maximum (FWHM) sizes as small as 70 ± 3 nm.

Motivated by the results shown in Fig. 4, we believe our experiment suffers from an unexplained transverse misalignment of the center of the coupling laser standing wave from the atomic cloud. To compensate for this, we simulate the experimental correlation traces by keeping the maximum power of the coupling laser standing wave as an adjustable parameter; there are no other fit parameters in these simulations. These simulation results are displayed in Figs. 6(c) and 6(d). We find that the two experimental traces are best captured when we assume a coupling laser power ranging from 0 to 3 mW [Figs. 6(c)] and 0 to 7.5 mW [Figs. 6(d)], respectively. With these assumed power ranges, there is good agreement between the experimental results and the numerical simulations. In particular, the shapes of the experimental traces are well reproduced in the simulations. Interestingly, the observed contrast of the experimental traces is slightly larger than what is predicted in the simulations.

We next discuss how we produce the simulated correlation traces that are displayed in Fig. 6. For the assumed power range of the coupling laser, we numerically solve the density matrix equations for the EIT pulse sequence at each point along the standing-wave spatial profile, generating the population transferred to the $F = 2$ level as a function of position. These transfer curves are displayed in Fig. 7. This spatial transfer pattern is convoluted with a copy of itself at different spatial offsets of the standing wave. During the time between the two EIT pulse sequences, the initial imprinted profile on the atoms spread out due to finite atomic temperature. We incorporate this spread by assuming a Gaussian Maxwell-Boltzmann velocity distribution of the atoms with the known temperature.

Since there is good agreement between the experimental results and the simulations of Fig. 6, we infer that the transfer profiles in Fig. 7 are a good reflection of what is achieved experimentally. For the 0 to 3 mW power range, the middle feature of Fig. 7(a) has a width of 97 nm or $\lambda/8$, which is a factor of 4 better than the diffraction limit. The 0 to 7.5 mW range transfer profile [Fig. 7(b)] has a width of 60 nm or $\lambda/13.3$, a factor of 6.6 better than the diffraction limit. The top plots in Fig. 7 show the calculated fidelity of the system to be in the dark state, $\mathrm{Tr}(\sqrt{\sqrt{\sigma}\rho\sqrt{\sigma}})$, using the same simulations of the density matrix. The fidelity drops to a low value of 33% near the nodes of the standing wave ("0" in the horizontal axis of the plots of Fig. 7) since coupling laser intensity vanishes at these points. The transfer profiles of Fig. 7 would be detrimental for quantum computing experiments since near the nodes there is substantial population in the excited level and therefore significant spontaneous emission and decoherence. As we will discuss below, the fidelity can be increased substantially by (i) operating near the single-photon resonance, and (ii) by off-setting the standing wave such that near the minima of the standing wave the coupling laser power drops to low values but does not vanish. The offset in the standing wave can be accomplished using a slight mismatch in the beam powers of the counterpropagating coupling lasers that form the standing wave.

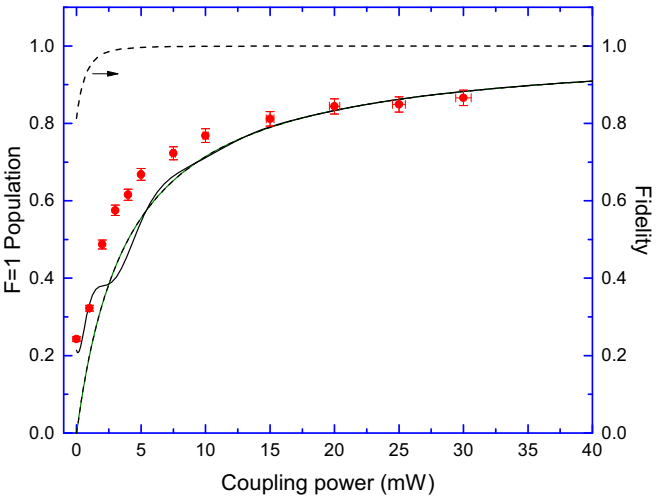

FIG. 8. (Color online) The population remaining in the $F = 1$ level after a single EIT pulse as the coupling laser power is varied. This experiment is performed using a single coupling beam and with the EIT lasers tuned to be resonant with the excited $F' = 2$ level. The solid black line is the result of numerical simulations of the density matrix without any adjustable parameters. The solid green line shows the $F = 1$ level population using the ideal dark state solution of Eq. (1). The dotted line is the fidelity of dark-state preparation, which quickly approaches unity for coupling laser power values above 2 mW. This experiment is performed with the atoms initially optically pumped into the $|F = 1, m = 0\rangle$ state; i.e., there is a single EIT channel. The calculated probe laser Rabi frequency is $\Omega_P = 5.78\Gamma$. For a coupling laser power of 40 mW, the calculated coupling Rabi frequency is $\Omega_C = 18.2\Gamma$.

V. ON-RESONANCE EXPERIMENTAL RESULTS

We next discuss our experiments when both the probe and coupling lasers of EIT are on single-photon resonance with the excited $F' = 2$ level. Being on resonance increases the interaction strength of the EIT lasers with the atomic system and reduces the nonadiabatic corrections to the dark state. In this experiment the probe size was decreased to a $1/e^2$ radius of 0.8 mm and its power was increased to 4 mW to raise its intensity. Increasing the probe laser intensity decreases the time required for the system to evolve into the dark state. The pulse widths for both the coupling and probe beams were kept the same, but the rise times of the pulses were increased by a factor of two (from about 20 ns to 40 ns). We found that increasing the rise times of the EIT beams in the simulations reduced nonadiabatic corrections to the dark state significantly. In these on-resonance experiments, to avoid complications from having three parallel m-level channels, we pump the atoms into the $|F = 1, m = 0\rangle$ state using an optical pumping beam. For this purpose, we apply a dc magnetic field of magnitude 3 G along the propagation direction of the EIT laser beams. The magnetic field defines the quantization axis and lifts the degeneracy of the m levels through the Zeeman shift. We then apply an additional laser which is

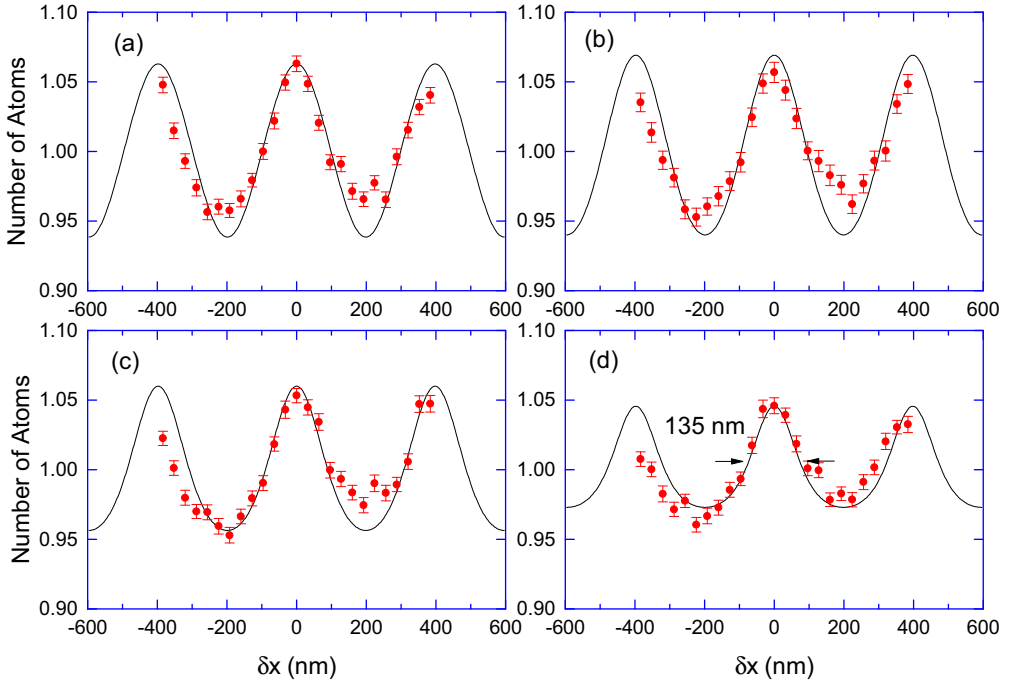

FIG. 9. (Color online) Experimental correlation traces for four different power ranges of the coupling laser standing wave: (a) 1 mW to 10 mW, (b) 1 mW to 20 mW, (c) 1 mW to 40 mW, and (d) 1 mW to 80 mW. The solid black lines are the results of simulations of the density matrix without any adjustable parameters. The calculated ranges for the coupling laser Rabi frequency are (a) 2.89Γ to 9.11Γ, (b) 2.89Γ to 12.9Γ, (c) 2.89Γ to 18.2Γ, and (d) 2.89Γ to 25.8Γ. The width of the trace in (d) is 135 ± 5 nm.

linearly polarized along the direction of the magnetic field. This laser pumps the atoms from the $|F = 1, m = \pm 1\rangle$ states into the $|F = 1, m = 0\rangle$ state via the $F' = 2$ excited level. The propagation direction of the optical pumping laser is roughly perpendicular to the FORT laser beam direction.

Figure 8 shows the population remaining in the $|F = 1, m = 0\rangle$ state using a single coupling laser as the coupling power is increased. For comparison, the black line shows the results of the numerical simulations of the density matrix and the green line is calculated using the ideal dark state solution of Eq. (1). The simulations of the density matrix are performed without any adjustable parameters. In contrast to the off-resonance results of Fig. 4, there is good agreement among experimental data, numerical simulations, and analytical solution. This is perhaps an indication of the robustness of the adiabatic preparation with respect to perturbations in experimental parameters. The dotted line in Fig. 8 is the calculated fidelity of the atomic system to be in the dark state. The fidelity quickly approaches unity for coupling laser power values above 2 mW.

We next discuss our correlation experiments with this set of experimental parameters (EIT beams tuned to single-photon resonance and atoms optically pumped to the $|F = 1, m = 0\rangle$ state at the start of the experiment). For these experiments, we set the counterpropagating beam powers such that the optical power of the coupling laser at the intensity minimum of the standing wave is 1 mW. This assures good overlap of the atomic system with the dark state at all points along the standing wave. Figure 9 shows the experimentally measured correlation traces for four different ranges of the standing wave: (a) 1 mW to 10 mW, (b) 1 mW to 20 mW, (c) 1 mW to 40 mW, and (d) 1 mW to 80 mW. The calculated ranges for the coupling laser Rabi frequency are (a) 2.89Γ to 9.11Γ, (b) 2.89Γ to 12.9Γ, (c) 2.89Γ to 18.2Γ, and (d) 2.89Γ to 25.8Γ, respectively. The solid black lines are the numerical simulations of the density matrix, again without any adjustable parameters. Unlike the off-resonance data in Fig. 6, the simulations in Fig. 9 show very good agreement with the contrast of the experimental data. The correlation traces do not have as much structure as the off-resonance results of Fig. 6 because of the good overlap with the dark state (i.e., the smooth nature of the transfer curve in Fig. 8). In fact, the fidelity never gets below 94% anywhere along the standing wave.

Figure 10 shows the inferred population transfer along the standing wave after a single EIT pulse for the four experimental conditions of Fig. 9. These population transfer results are used to generate the simulations of the correlation traces as shown in Fig. 9. In Fig. 10, we also plot the simulated fidelity along one period of the standing wave. As the intensity of the standing wave increases the atoms are transferred to $F = 2$ in ever smaller regions. For coupling power range of 1 to 80 mW, Fig. 10(d) shows that the transfer is localized to a region with a width of 70 nm, which is a factor of 11.3 times smaller than the wavelength of the coupling and probe lasers.

VI. HEISENBERG UNCERTAINTY LIMIT OF THE MEASUREMENT PROTOCOL

In this section, we discuss a fundamental limitation of the smallest feature size that can be measured using our correlation protocol. In our measurements we apply two EIT pulse sequences separated by a certain time delay (1.5 μs for

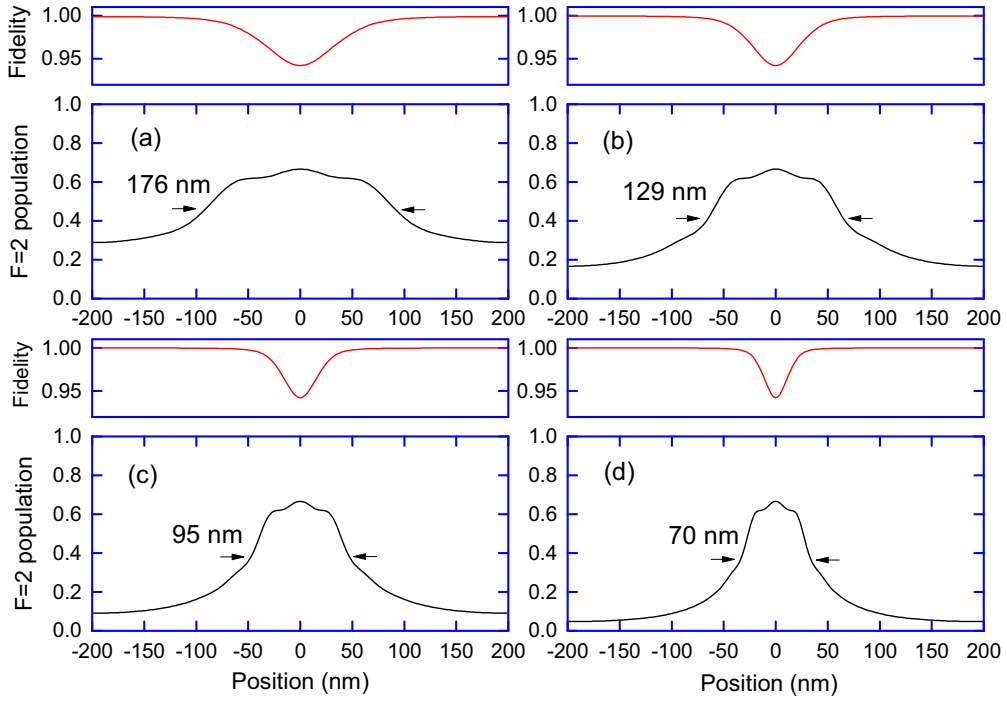

FIG. 10. (Color online) The inferred population transfer to the $F = 2$ level as a function of the position in the standing wave for coupling power ranges the same as those displayed in Fig. 9. "0" in the horizontal axis coincides with the intensity minimum of the standing wave and the results are displayed over one period. These simulated features produce the correlation traces that match the experimental results as shown in Fig. 9. In (d) (coupling laser power range of 1 to 80 mW), the transfer is localized to a region with a width of 70 nm, which is a factor of 11.3 times smaller than the wavelength of the coupling and probe beams. The top plots show the calculated fidelity of the system to be in the dark state. The fidelity is above 94% at all points along the standing wave.

the experiments that we presented in this paper), and it is critical that the atoms do not move substantially during this time. Even at very low atomic temperatures, there will be a momentum spread induced in the atoms due to measurement-induced localization of the atomic wave function. After the first EIT pulse sequence, but before the blow-away beam is turned on, the probability of finding an atom is uniform across the standing wave (i.e., there is no spatial structure of the position of the atom). The blow-away beam projects the wave function of the atoms that remain in the trap to the $F = 1$ level, and imprints the spatial structure with tightly localized features. Because of Heisenberg's uncertainty principle, this spatial localization inevitably entails a spread in the momentum distribution of the atoms. This momentum (velocity) distribution would cause a spread of the transfer profile between the two EIT pulse sequences, blurring the correlation features. Following the work of Agarwal and colleagues [29], we model the momentum distribution of the atoms over one period of the standing wave using

$$\mathscr{P}_1(p) = |\langle p, F = 1|\Psi_{\text{dark}}\rangle|^2 = \left|\int_{-\pi}^{\pi} \sqrt{\rho_{11}(x)}e^{ipx}dx\right|^2. \quad (2)$$

Here p denotes the atomic momentum and the quantity $\rho_{11}(x)$ is the probability of finding the atom in the $F = 1$ level as a function of position after the first EIT pulse. For a given set of EIT parameters, we can use the transfer profiles from our simulations and then calculate the momentum distribution of the atoms between the two EIT pulses using Eq. (2). The smallest time between the two EIT pulses is limited to 1.5 μs, since this is the time required to heat the atoms that have been transferred to the $F = 2$ level from the trap. Using this procedure, we calculate that the Heisenberg limit sets the smallest feature size that can be measured to be 20 nm. This shows that the experiments we have presented in this paper are not limited by this effect. However, for future experiments, demonstrating feature sizes smaller than 20 nm would require a measurement protocol that is substantially different from our correlation experiments.

VII. CONCLUSIONS

In conclusion, we have reported a detailed investigation of localization of excitation using the dark state of EIT. We experimentally transferred atoms between hyperfine levels of ultracold ^{87}Rb atoms within a spatial width of 70 nm, which is a factor of 11.3 times smaller than the wavelength of the lasers used to perform the transfer. This was achieved using 150-ns-long EIT pulses and with an inferred dark-state preparation fidelity exceeding 94% throughout the standing wave. We have also inferred feature sizes as small as 60 nm, but for those parameters the fidelity of dark-state preparation was poor. As we discussed above, the dark-state-based approach has unique advantages that may be especially useful for quantum computing experiments in which nanoscale-level addressing with little decoherence is required. An exciting future direction

is to implement subwavelength spatial resolution single-qubit and two-qubit gates. As discussed in detail in Ref. [31], the dark-state-based localization can be combined with additional coherent excitations to perform gates with nanometer spatial resolution.

ACKNOWLEDGMENTS

We thank Nick Brewer and David Gold for many helpful discussions. We also would like to thank the Air Force Office of Scientific Research (AFOSR) and the University of Wisconsin–Madison for financial support.

[1] M. A. Nielsen and I. L. Chuang, *Quantum Computation and Quantum Information* (Cambridge University Press, Cambridge, 2000).

[2] E. Urban, T. A. Johnson, T. Henage, L. Isenhower, D. D. Yavuz, T. G. Walker, and M. Saffman, Observation of Rydberg blockade between two atoms, Nat. Phys. **5**, 110 (2009).

[3] L. Isenhower, E. Urban, X. L. Zhang, A. T. Gill, T. Henage, T. A. Johnson, T. G. Walker, and M. Saffman, Demonstration of a Neutral Atom Controlled-NOT Quantum Gate, Phys. Rev. Lett. **104**, 010503 (2010).

[4] A. Gaetan, Y. Miroshnychenko, T. Wilk, A. Chotia, M. Viteau, D. Comparat, P. Pillet, A. Browaeys, and P. Grangier, Observation of collective excitation of two individual atoms in the Rydberg blockade regime, Nat. Phys. **5**, 115 (2009).

[5] T. Wilk, A. Gaetan, C. Evellin, J. Wolters, Y. Miroshnychenko, P. Grangier, and A. Browaeys, Entanglement of Two Individual Neutral Atoms Using Rydberg Blockade, Phys. Rev. Lett. **104**, 010502 (2010).

[6] M. O. Scully and M. S. Zubairy, *Quantum Optics* (Cambridge University Press, Cambridge, 1997).

[7] S. E. Harris, Electromagnetically induced transparency, Phys. Today **50**(7), 36 (1997).

[8] O. Kocharovskaya, Amplification and lasing without inversion, Phys. Rep. **219**, 175 (1992).

[9] M. Fleischhauer, A. Imamoglu, and J. P. Marangos, Electromagnetically induced transparency: Optics in coherent media, Rev. Mod. Phys. **77**, 633 (2005).

[10] S. W. Hell, Far-field optical nanoscopy, Science **316**, 1153 (2007).

[11] P. C. Maurer, J. R. Maze, P. L. Stanwix, L. Jiang, A. V. Gorshkov, A. A. Zibrov, B. Harke, J. S. Hodges, A. S. Zibrov, A. Yacoby, D. Twitchen, S. W. Hell, R. L. Walsworth, and M. D. Lukin, Far-field optical imaging and manipulation of individual spins with nanoscale resolution, Nat. Phys. **6**, 912 (2010).

[12] J. E. Thomas, Uncertainty limited position measurement of moving atoms using optical fields, Opt. Lett. **14**, 1186 (1989).

[13] J. E. Thomas, Quantum theory of atomic position measurement using optical fields, Phys. Rev. A **42**, 5652 (1990).

[14] K. D. Stokes, C. Schnurr, J. R. Gardner, M. Marable, G. R. Welsch, and J. E. Thomas, Precision Position Measurement of Moving Atoms Using Optical Fields, Phys. Rev. Lett. **67**, 1997 (1991).

[15] J. R. Gardner, M. L. Marable, G. R. Welsch, and J. E. Thomas, Suboptical Wavelength Position Measurement of Moving Atoms Using Optical Fields, Phys. Rev. Lett. **70**, 3404 (1993).

[16] F. Le Kien, G. Rempe, W. P. Schleich, and M. S. Zubairy, Atom localization via Ramsey interferometry: A coherent cavity field provides a better resolution, Phys. Rev. A **56**, 2972 (1997).

[17] S. Qamar, S. Y. Zhu, and M. S. Zubairy, Atom localization via resonance fluorescence, Phys. Rev. A **61**, 063806 (2000).

[18] K. T. Kapale, S. Qamar, and M. S. Zubairy, Spectroscopic measurement of an atomic wave function, Phys. Rev. A **67**, 023805 (2003).

[19] M. Sahrai, H. Tajalli, K. T. Kapale, and M. S. Zubairy, Subwavelength atom localization via amplitude and phase control of the absorption spectrum, Phys. Rev. A **72**, 013820 (2005).

[20] M. Macovei, J. Evers, C. H. Keitel, and M. S. Zubairy, Localization of atomic ensembles via superfluorescence, Phys. Rev. A **75**, 033801 (2007).

[21] J. T. Chang, J. Evers, M. O. Scully, and M. S. Zubairy, Measurement of the separation between atoms beyond diffraction limit, Phys. Rev. A **73**, 031803(R) (2006).

[22] E. Paspalakis and P. L. Knight, Localizing an atom via qauntum interference, Phys. Rev. A **63**, 065802 (2001).

[23] J. Xu and X. Hu, Sub-half-wavelength localization of an atom via trichromatic phase control, J. Phys. B: At. Mol. Opt. Phys. **40**, 1451 (2007).

[24] P. Storey, M. Collett, and D. Walls, Measurement Induced Diffraction and Interference of Atoms, Phys. Rev. Lett. **68**, 472 (1992).

[25] R. Quadt, M. Collett, and D. Walls, Measurement of Atomic Motion in a Standing Light Field by Homodyne Detection, Phys. Rev. Lett. **74**, 351 (1995).

[26] S. Kunze, K. Dieckmann, and G. Rempe, Diffraction of Atoms from a Measurement Induced Grating, Phys. Rev. Lett. **78**, 2038 (1997).

[27] M. Holland, S. Marksteiner, P. Marte, and P. Zoller, Measurement Induced Localization from Spontaneous Decay, Phys. Rev. Lett. **76**, 3683 (1996).

[28] C. Weitenberg, M. Endres, J. F. Sherson, M. Cheneau, P. Schauss, T. Fukuhara, I. Bloch, and S. Kuhr, Single-spin addressing in an atomic Mott insulator, Nature (London) **471**, 319 (2011).

[29] G. S. Agarwal and K. T. Kapale, Subwavelength atom localization via coherent population trapping, J. Phys. B: At. Mol. Opt. Phys. **39**, 3437 (2006).

[30] D. D. Yavuz and N. A. Proite, Nanoscale resolution fluorescence microscopy using electromagnetically induced transparency, Phys. Rev. A **76**, 041802(R) (2007).

[31] A. V. Gorshkov, L. Jiang, M. Greiner, P. Zoller, and M. D. Lukin, Coherent Quantum Optical Control with Sub-wavelength Resolution, Phys. Rev. Lett. **100**, 093005 (2008).

[32] J. Choi and D. S. Elliott, Influence of interaction time and population redistribution on the localization of atomic excitation through electromagnetically induced transparency, Phys. Rev. A **89**, 013414 (2014).

[33] H. Li, V. A. Sautenkov, M. M. Kash, A. V. Sokolov, G. R. Welch, Y. V. Rostovtsev, M. S. Zubairy, and M. O. Scully, Optical imaging beyond the diffraction limit via dark states, Phys. Rev. A **78**, 013803 (2008).

[34] N. A. Proite, Z. J. Simmons, and D. D. Yavuz, Observation of atomic localization using electromagnetically induced transparency, Phys. Rev. A **83**, 041803(R) (2011).

[35] J. A. Miles, Z. J. Simmons, and D. D. Yavuz, Subwavelength Localization of Atomic Excitation Using Electromagnetically Induced Transparency, Phys. Rev. X **3**, 031014 (2013).

[36] B. E. Unks, N. A. Proite, and D. D. Yavuz, Generation of high-power laser light with GHz splitting, Rev. Sci. Instrum. **78**, 083108 (2007).

[37] D. A. Steck, Rubidium 87 D line data, available online at http://steck.us/alkalidata (revision 2.1.4, 23 December 2010).